Investigation of the Production of ^{152}Tb and ^{155}Tb Terbium Radioisotopes with Europium Targets

C. Yalçın[1, *]

[1]*Kocaeli University, Department of Physics, Umuttepe 41001, Kocaeli, Turkey*

In recent years, terbium radioisotopes have been investigated for their potential therapeutic and diagnostic applications in nuclear medicine. This study aimed to investigate the production of ^{152}Tb and ^{155}Tb by alpha induced reaction in detail, with a specific focus on determining the optimum production parameters and testing existing nuclear models. Given the limited number of experiments conducted on reactions related to terbium isotope production, it is necessary to perform theoretical calculations of cross sections over a wide energy range in order to gain a detailed understanding of terbium isotope production. In order to achieve this objective, the cross sections of the ^{151}Eu(α,n)^{154}Tb reactions were calculated up to 60 MeV using the TALYS computer code with 432 different combinations of optical model parameters, level density, and strength function models. The theoretical reaction cross section results were compared with the experimental results in the literature. The best input parameters were determined using the Threshold Logic Unit method and these parameters were used in all isotope production calculations. Once the optimal model combination had been determined, the total activity production and isotopic fraction of ^{152}Tb and ^{155}Tb isotopes were calculated in detail for beam energies of 17-50 MeV, different irradiation times, and varying ^{151}Eu and ^{153}Eu target thicknesses.

Keywords: Terbium radioisotopes, Medical isotope production, Alpha induced reactions, Cross section, Threshold Logic Unit method

I. INTRODUCTION

A multitude of medical radioisotopes, including ^{18}F, ^{99m}Tc, ^{68}Ga, and ^{177}Lu, are currently utilized for diagnostic and therapeutic purposes. However, in recent years, novel radioisotopes have been proposed that exhibit numerous advantages over existing radioisotopes. In particular, the utilization of radiolanthanides in nuclear medicine has been the subject of numerous in vitro and in vivo studies [1]. In a recent preclinical study, Müller et al. [2] investigated the combined use of ^{149}Tb, ^{152}Tb, ^{155}Tb, and ^{161}Tb radioisotopes. These radionuclides are distinctive in that they exhibit properties suitable for positron emission tomography (PET), single−photon emission computed tomography (SPECT), and radionuclide therapy, the three principal modalities of nuclear medicine. Müller et al. employed a folate-based targeting agent comprising a dodecane tetraacetic acid (DOTA) chelator to facilitate the binding of Tb to the biomolecule, and reported highly promising results [2]. Imaging of folate receptor (FR) positive human tumors xenografted into mice with both ^{152}Tb (PET, 17% β^+) and ^{155}Tb (SPECT) has been demonstrated to be of high quality. Furthermore, the same compound, labeled with therapeutic ^{149}Tb and ^{161}Tb, demonstrated the potential to cure the disease.

The primary production method for ^{161}Tb is irradiation of ^{160}Gd with thermal neutrons in a reactor [3]. The production of ^{149}Tb, ^{152}Tb, and ^{155}Tb may be accomplished via charged particle accelerators. An overview of ^{149}Tb production methods can be found in [4–7], while an overview of ^{155}Tb production methods can be found in [8]. The production of ^{152}Tb can be achieved through the irradiation of Gd and Eu isotopes with protons [9–11], deuterons [12] and alphas [13, 14], as well as spallation reactions initiated by high energy protons [15].

Although there have been a certain number of experimental studies on the production of medical terbium isotopes, the appropriate production mechanism has not yet been fully proposed. In cases where experimental studies are not sufficient, the combination of theoretical investigation with experiments can be a helpful approach. To study isotope production theoretically, the reaction cross sections in the region of interest must be well known. The theoretical cross sections can be calculated using the Hauser Feshbach statistical model. In these calculations, parameters such as the optical model, level densities, and strength function are employed. As these parameters have not yet been determined globally, they vary according to the mass and energy region of interest. All of these models have an impact on the theoretical cross section calculations, particularly in the low-energy region, where the optical α+nucleus potential is likely to introduce the most significant deviations in the charged particle reactions [16–19]. The parameters proposed thus far are presented in Tables 1, 2, and 3. Consequently, it is essential to determine which models should be utilized for theoretical cross section calculations. In order to ascertain which models are most appropriate for use in the region of interest, the ^{151}Eu(α,n)^{154}Tb reaction cross section was subjected to a detailed analysis and compared with the experimental results of Gyürky et al. [13], which exhibit the lowest energy and cross section uncertainties. A total of 432 different combinations of eight optical potentials, six level densities, and nine strength function models were subjected to reaction cross section calculations, which were then compared with experimental results. Threshold Logic Unit method [16, 20] was used to determine the best model parameters.

In the present study, the cross sections of the alpha induced reactions of ^{151}Eu(α,3n)^{152}Tb and ^{151}Eu(α,2n)^{153}Tb and ^{151}Eu(α,n)^{154}Tb and ^{153}Eu(α,2n)^{155}Tb were calculated with best model parameters for the production of ^{152}Tb and ^{155}Tb. Optimal production parameters for ^{152}Tb and ^{155}Tb have been proposed for commercial cyclotron accelerators. This work can be studied not only in the medical physics, but

* E-mail: caner.yalcin@kocaeli.edu.tr

also in other fields where knowledge of reaction cross sections is required, such as nuclear astrophysics [16, 21–25] and nuclear technology [26].

II. METHOD AND CALCULATION

A. Cross Section Calculations

The cross sections for the ^{151}Eu(α,n)^{154}Tb reaction were predicted using the TALYS 1.96 computer code [27], which employs Hauser Feshbach statistical model calculations. Optical model potentials (OMP), level density models (LDM), and strength function models (SFM) play a significant role in the theoretical cross section calculations. For further details regarding the models, please refer to the relevant references. In order to investigate the sensitivities of these parameters to reaction cross sections, calculations were performed for combinations of eight OMP, six LDM, and nine SFMs, as presented in Tables 1, 2, and 3. Once the optimal model had been identified, the reaction pathways illustrated in Figure 1 and the synthesis of ^{152}Tb and ^{155}Tb were subjected to further analysis.

Table 1. Optical model potentials (OMP), which are available in the Talys code. The default options for OMP is the Avrigeanu et al. (2014) (OMP-6)[31].

Model no	Optical model potential
OMP-1	Normal alpha potential (1958) [28]
OMP-2	McFadden and Satchler (1966) [29]
OMP-3	Demetriou et al. (2002) (table 1) [30]
OMP-4	Demetriou et al. (2002) (table 2) [30]
OMP-5	Demetriou et al. (2002) (dispersive model) [30]
OMP-6	Avrigeanu et al. (2014) [31]
OMP-7	Nolte et al. (1987) [32]
OMP-8	Avrigeanu et al. (1994) [33]

Table 2. Level density models(LDM) which are available in the Talys code. The default options for LDM is constant temperature + Fermi gas model (LDM-1) [34].

Model no	Level density model
LDM-1	Constant temperature + Fermi gas model [34]
LDM-2	Back-shifted Fermi gas model [35, 36]
LDM-3	Generalised superfluid model [37, 38]
LDM-4	Microscopic level densities (Skyrme force) [39] from Goriely's tables
LDM-5	Microscopic level densities (Skyrme force) [40] from Hilaire's combinatorial tables
LDM-6	Microscopic LD (temp. dependent HFB, Gogny force) from Hilaire's combinatorial tables (2014) [41]

The OMPs is major input parameter for the calculation of cross section. The OMPs used in the calculations, labeled with OMP-1 through OMP-8, are normal alpha potential [28], McFadden and Satchler [29], Demetriou et al. [30] , Avrigeanu et al. [31] which is the default option of the code, Nolte et al. [32], Avrigeanu et al. [33].

Table 3. Gamma-ray strength function models (SFM) which are available in the Talys code. The default options for SFM is the Brink-Axel Lorentzian model (SFM-2) [44, 45].

Model no	Strength function model
SFM-1	Kopecky-Uhl generalized Lorentzian [42, 43]
SFM-2	Brink-Axel Lorentzian [44, 45]
SFM-3	Hartree-Fock BCS tables [46]
SFM-4	Hartree-Fock-Bogolyubov tables [47]
SFM-5	Goriely's hybrid model [48]
SFM-6	Goriely T-dependent HFB [51]
SFM-7	T-dependent RMF [49]
SFM-8	Gogny D1M HFB+QRPA [50]
SFM-9	Simplified Modified Lorentzian (SMLO) [52]

Three microscopic and three phenomenological level density models were included in the calculations. The phenomenological LDMs are constant temperature + Fermi gas model [34], back-shifted Fermi gas model [35, 36] and generalized super-fluid model [37, 38], labeled with LDM-1 through LDM-3. Two microscopic LDMs were chosen using Skyrme force from Goriely's (LDM-4) [39] and Hilaire's (LDM-5) [40] tables. The third microscopic LDM used Gogny force from Hilaire's combinatorial tables (LDM-6) [41]. The default option of the code is Constant Temperature - Fermi Gas Model (LDM-1) [34].

Nine different SFMs were chosen in the calculations, labeled with SFM-1 through SFM-9, given in Table 3. The default option of the SFM is the Brink-Axel Lorentzian model (SFM-2) [44, 45].

B. Threshold Logic Unit Method

In order to identify the most compatible input parameter sets, the threshold logic unit (TLU) method was employed to evaluate 432 combinations of eight OMP, six LDM, and nine SFMs for the alpha-induced reaction of the ^{151}Eu isotope. The TLU method is founded upon the concept of a binary threshold function. In this approach, each input is multiplied by a weight, and the sum of these weighted inputs is compared to a threshold value, as expressed in Eq. (2) and referenced in [20]. If the sum exceeds the threshold, the TLU outputs a 1; otherwise, it outputs a 0.

In this study, the input values (X_i) are determined by comparing the TALYS results with the experimental values within twice their uncertainties, as

$$X_i = \begin{cases} 1 & \text{if} \quad \sigma_{Ei} - 2\Delta\sigma_{Ei} \leq \sigma_{Ti} \leq \sigma_{Ei} + 2\Delta\sigma_{Ei} \\ 0 & \text{otherwise} \end{cases} \qquad (1)$$

where, σ_{Ei}, and σ_{Ti} are the experimental and TALYS results, respectively, and $\Delta\sigma_{Ei}$ is the experimental uncertainty, at energy i.

The obtained binary input values were compared with the

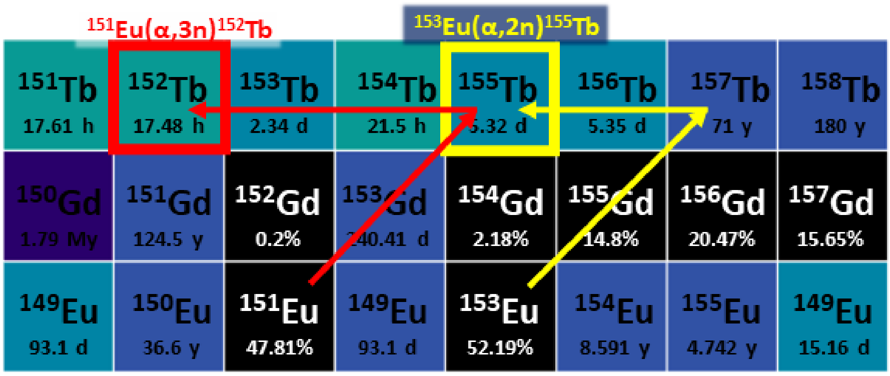

Fig. 1. (Color online) The relevant part of the isotope table and the production route to be used for the production of the medical isotopes ^{152}Tb and ^{155}Tb [53].

threshold τ and the best model combinations BMC were determined, as

$$BMC = \begin{cases} 1 & \text{if } \sum_{i=1}^{n}(\theta_i X_i) \geq \tau \\ 0 & \text{otherwise} \end{cases} \tag{2}$$

here, the weight factors (θ_i) are taken as one since weights of the cross sections are equal at all energies, n is the number of the energies at which the experiments were carried out, and the threshold τ is selected as the number of experimental energies at which the TALYS results were accepted with the experimental values within twice their uncertainties, that is X_i is one, otherwise X_i is zero. The cross sections of the ^{151}Eu(α,n)^{154}Tb reaction were measured at thirteen different energies, indicating that n is equal to thirteen. The TLU method was then applied for three threshold values, namely, τ = 11, 12, and 13. The calculation of medical isotope production was performed using the TALYS results, with the objective of identifying the optimal combination of models that were in accordance with the experimental values at all twelve energies. This process revealed that the threshold was twelve.

Table 4. The production route and properties of the isotopes under investigation [53].

Isotope	$T_{1/2}$	Reaction	Q-value (MeV)	Decay Mode
^{150}Tb	3.48 h	^{151}Eu(α,5n)^{150}Tb	-41.48	$\epsilon + \beta^+$ (100%)
^{151}Tb	17.61 h	^{151}Eu(α,4n)^{151}Tb	-32.89	$\epsilon + \beta^+$ (99.9905%) α (0.0095%)
^{152}Tb	16.48 h	^{151}Eu(α,3n)^{152}Tb	-25.72	$\epsilon + \beta^+$ (100%)
^{153}Tb	2.34 d	^{151}Eu(α,2n)^{153}Tb	-17.06	$\epsilon + \beta^+$ (100%)
^{154g}Tb	21.5 h	^{151}Eu(α,n)^{154g}Tb	-10.14	$\epsilon + \beta^+$ (100%)
^{154m1}Tb	9.99 h	^{151}Eu(α,n)^{154m1}Tb	-10.26	$\epsilon + \beta^+$ (78.2%) IT (21.8%)
^{154m2}Tb	22.7 h	^{151}Eu(α,n)^{154m2}Tb	-10.54	$\epsilon + \beta^+$ (98.2%) IT (1.8%)
^{154g}Tb	21.5 h	^{153}Eu(α,3n)^{154g}Tb	-25.00	$\epsilon + \beta^+$ (100%)
^{154m1}Tb	9.99 h	^{153}Eu(α,3n)^{154m1}Tb	-25.11	$\epsilon + \beta^+$ (100%) IT (21.8%)
^{154m2}Tb	22.7 h	^{153}Eu(α,3n)^{154m2}Tb	-25.40	$\epsilon + \beta^+$ (100%) IT (1.8%)
^{155}Tb	5.32 d	^{153}Eu(α,2n)^{155}Tb	-15.97	ϵ (100%)
^{156}Tb	5.35 d	^{153}Eu(α,n)^{156}Tb	-9.31	$\epsilon + \beta^+$ (100%)

C. Production of Terbium Radioisotopes

Once the most suitable model had been selected, the reaction pathways depicted in Figure 1, along with the production of ^{152}Tb and ^{155}Tb, were calculated with the Talys code. The total number of the produced nuclei $Y(t)$ during an irradiation time t (t=0 at the beginning of irradiation) is given by following equation [54]

$$\begin{aligned} Y(t) &= t\int_0^L \mathrm{d}x I(x)\sigma(x)\left(\frac{\rho}{Ze}\right) \\ &\cong tI_0 \int_{E_{back}}^{E_{beam}} \mathrm{d}E \left(-\frac{1}{\rho}\frac{dE}{dx}\right)^{-1}\frac{\sigma(E)}{Ze} \\ &\equiv tI_0 y \end{aligned} \tag{3}$$

where ρ is the target isotope number density, L is the target thickness, I_0 is the number of beam particles irradiating the sample per unit irradiation time, Z is the charge number and e is the electron charge. E_{beam} denotes the incident beam energy and E_{back} is the average projectile energy available at the backside of the target. Cross section to produce the isotope at depth x in the sample is $\sigma(x)$, and $-(1/\rho)(dE/dx)$ is the stopping power. The y term is the number of the produced nuclei following deposition of unit induced electric charge.

If the projectiles travels through the target, the average projectile beam energy will decrease. The amount of energy loss inside the target is determined by the target thickness and the stopping power. The Talys code calculates the stopping power using the Bethe-Bloch formula [55]. The integration limits E_{beam} and E_{back} are fixed by the requested projectile energy range inside the target, which is determined by the cross section as function of projectile energy. The spreading of the beam inside the target is neglected. The stopping power describes the average energy loss of projectiles in the target by atomic collisions as a function of their energy in (MeV/cm).

III. RESULTS AND DISCUSSION

In order to study the production of terbium isotopes, it is essential to have a comprehensive understanding of the relevant experimental and theoretical cross sections within the designated energy range. It is regrettable that not all cross sections necessary for the production of terbium isotopes have been experimentally measured at the relevant energies. Consequently, theoretical cross sections may prove an efficacious instrument for the investigation of radioisotope production. Nevertheless, the accuracy of calculated theoretical cross sections is not guaranteed, particularly in the case of alpha-initiated reactions. A multitude of parameters are employed in the calculation of cross sections. Therefore, it is essential to examine each parameter individually for each nucleus and energy range. In order to ascertain which models are most appropriate for use in the region of interest, the ^{151}Eu(α,n)^{154}Tb reaction cross section was subjected to a detailed analysis and compared with the experimental results of Gyürky et al. [13], which exhibit the lowest energy and cross section uncertainties. A total of 432 different combinations of eight optical potentials, six level densities, and nine power function models were subjected to reaction cross section calculations, which were then compared with experimental results. Threshold Logic Unit method [16, 20] was used to determine the best model parameters.

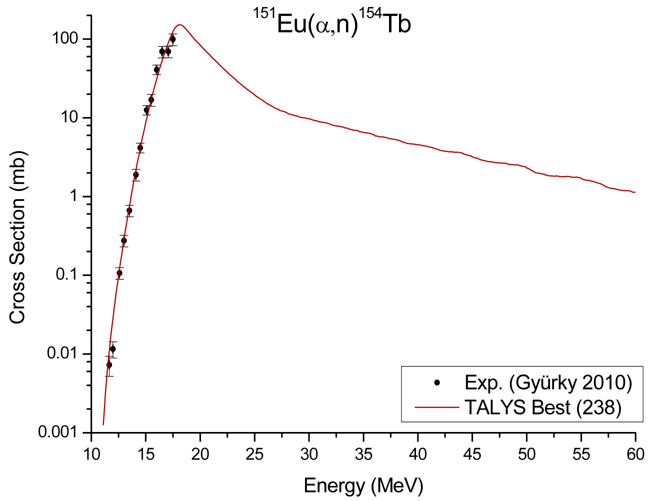

Fig. 2. (Color online) The ^{151}Eu(α,n)^{154}Tb cross sections obtained by TALYS using the best combination (MP-238) selected. The first digit in the legend represents the Optical Model number, the second digit the Level Density model number and the third digit the Strength Function model number (Table 1, 2, and 3).

The theoretical results of the ^{151}Eu(α,n)^{154}Tb reaction cross section were calculated with 432 combinations of eight OMP, six LDM, and nine SFM were compared with experimental values [13] measured at thirteen energies. Model Parameters are labeled with $MP-ijk$, where i, j and k represent $OMP-i$, $LDM-j$ and $SFM-k$, respectively, in Tables 1, 2, and 3. In the study employing the TLU method, the optimal combinations (MP-238) were identified that were in alignment with the experimental results at twelve energies of the thirteen, as illustrated in Fig. 2. The calculated cross section values are in agreement with the experiment at all points except the 11.99 MeV energy point. Additionally, the calculated and experimental cross section values can be found in Table 5.

Table 5. Cross Sections calculated with MP-238, and experimental values, for ^{151}Eu(α,n)^{154}Tb reaction.

$E_{Lab.}$ (MeV)	TALYS (MP-238) mb	Experiment[a] mb
11.65 ± 0.04	0.011	0.007 ± 0.002
11.99 ± 0.04	0.029	0.012 ± 0.003
12.59 ± 0.04	0.120	0.11 ± 0.02
13.00 ± 0.04	0.287	0.276 ± 0.047
13.50 ± 0.04	0.758	0.666 ± 0.111
14.10 ± 0.04	2.173	1.898 ± 0.322
14.50 ± 0.04	4.134	4.169 ± 0.580
15.09 ± 0.04	9.829	12.583 ± 1.733
15.51 ± 0.05	17.193	16.932 ± 2.904
16.00 ± 0.05	31.056	41.008 ± 5.759
16.50 ± 0.05	52.976	69.274 ± 11.793
17.07 ± 0.05	89.319	69.490 ± 11.750
17.50 ± 0.05	124.821	99.486 ± 17.256

[a]Ref. [13].

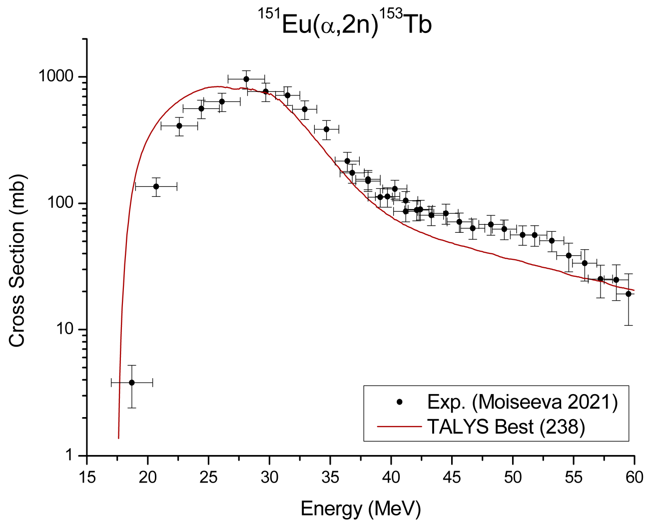

Fig. 3. (Color online) The ^{151}Eu(α,2n)^{153}Tb cross sections obtained by TALYS using the best combination. The explanations same as in Fig. 2.

Furthermore, the model was tested for the medical isotope production reactions, specifically the ^{151}Eu(α,2n)^{153}Tb and the ^{151}Eu(α,3n)^{152}Tb reactions. As illustrated in Figures 3 and 4, the outcomes produced by the MP-238 model are in alignment with the experimental findings reported by Moiseeva et al [14]. Unfortunately, there are no experimental measurements in the literature for the ^{153}Eu(α,2n)^{155}Tb reaction used for ^{155}Tb production. Consequently, the theoretical cross sections could not be compared with the experimental results. For these reactions, MP-238 was assumed to be

compatible due to the close mass and properties of the target isotopes of Eu, and this model combination was used in all isotope production calculations.

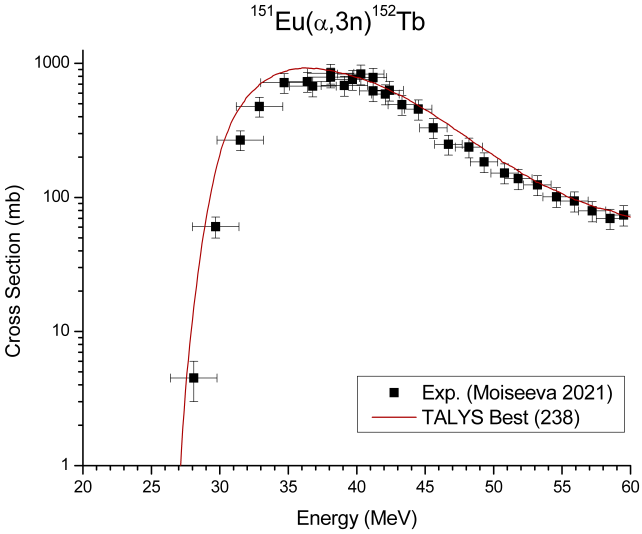

Fig. 4. (Color online) The ^{151}Eu(α,3n)^{152}Tb cross sections obtained by TALYS using the best combination. The explanations same as in Fig. 2.

A. The production of ^{152}Tb with ^{151}Eu target

For the production calculation of ^{152}Tb, it was assumed that the enriched ^{151}Eu target was irradiated with an alpha beam in 1 MeV steps starting at 30 MeV up to 50 MeV and the activities and isotopic fractions of the isotopes produced in all reaction channels were calculated. A comprehensive analysis was conducted to ascertain the impact of irradiation time on the calculated values, spanning from one to 24 hours. Additionally, the influence of varying target thicknesses on the results was investigated, providing insights into the effect of these variables on the observed outcomes. The results obtained with 8 hours of irradiation are given in Figures 5 and 6. As Europium is typically present in its oxide form and is known to undergo rapid oxidation, this study employs the assumption that the Eu target is in its oxide form throughout the calculations.

As can be seen in Figure 6, with a beam energy of 50 MeV and a target thickness corresponding to an output energy of 34 MeV (corresponding to a 0.26 mm thick target), ^{152}Tb with an isotopic fraction of 0.83 can be produced in 8 hours with an activity of 395 MBq/μA (Figure 5). As the exit energy decreases below 34 MeV, a notable decline in the isotopic fraction and radionuclide purity is observed, as illustrated in Figure 6. As the irradiation time is extended, the ^{152}Tb fraction is calculated to decrease by about 1% every eight hours.

Moiseeva et al. [14] proposed the production of ^{152}Tb with a 42 MeV beam current and 34 MeV beam exit energy. However, as illustrated in the Figures 5 and 6, both the isotopic fraction and activity increase in ^{152}Tb production with

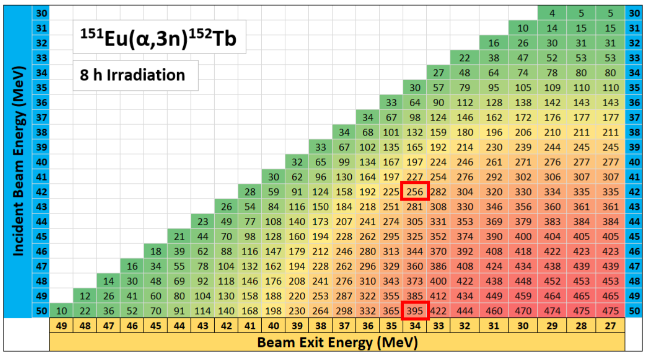

Fig. 5. (Color online) The activity of ^{152}Tb (in MBq/μA) is presented as a function of beam energy and target thickness at a beam current of 1 μA and an irradiation time of 8 h with an enriched ^{151}Eu target. The target thickness is expressed in terms of beam exit energy, and the beam profile is assumed to be 1 cm^2.

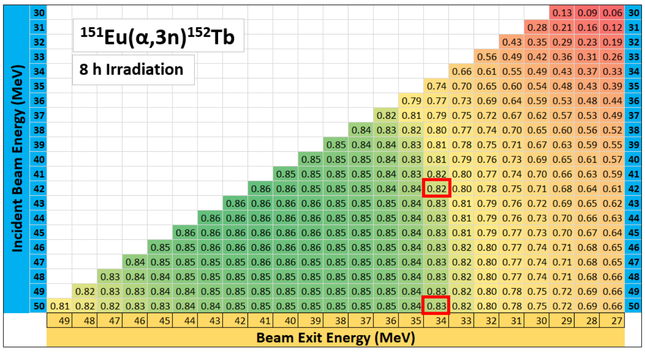

Fig. 6. (Color online) The isotopic fraction of ^{152}Tb with respect to beam energy and target thickness was determined following irradiation with an enriched ^{151}Eu target at a beam current of 1 μA for 8 hours. The target thickness is expressed in terms of the beam energy leaving the target. The beam profile was assumed to be 1 cm^2.

50 MeV beam energy and 34 MeV exit energy. While the isotopic fraction shows only a modest increase, the activity level rises significantly, from 256 to 395 MBq/μA. Furthermore, our calculations, based on the combination proposed by Moiseeva et al.[14], are in accordance with the experimental findings. The activity reported by Moiseeva et al.[14], 222 MBq/μA, was calculated to be 256 MBq/μA. Figure 7 illustrates the variation in isotopic fractions as a function of target thickness when irradiated with 50 MeV (solid line) and 42 MeV (dashed line) beams. As evidenced by the region highlighted in yellow in the graph, the isotopic fraction exhibits minimal change for ^{152}Tb up to an exit energy of 34 MeV. Figure 8 illustrates the impact of varying target thicknesses on the produced activity when irradiated with 50 MeV and 42 MeV beams. The threshold energy for the ^{151}Eu(α,4n)^{151}Tb reaction is 33.76 MeV. Therefore, the production of ^{151}Tb is not possible at energies below the threshold. In the same way, ^{150}Tb, which results from the ^{151}Eu(α,5n)^{150}Tb reaction, cannot be produced below the threshold energy of 42,6 MeV. For this reason, Figure 8 presents only the activity produced by irradiation with a 50 MeV energy beam. The maxi-

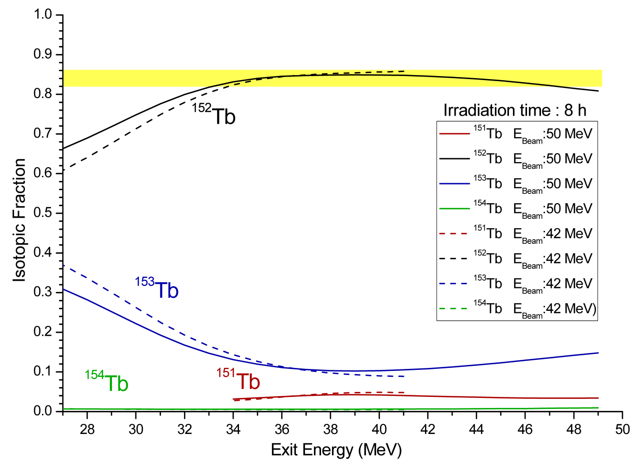

Fig. 7. (Color online) 1 μA beam current and 8 hours of irradiation with 42 MeV (dashed line) and 50 MeV (solid line) beam energy and ^{152}Tb isotopic fraction with respect to target thickness. Target thickness is given in terms of beam exit energy.

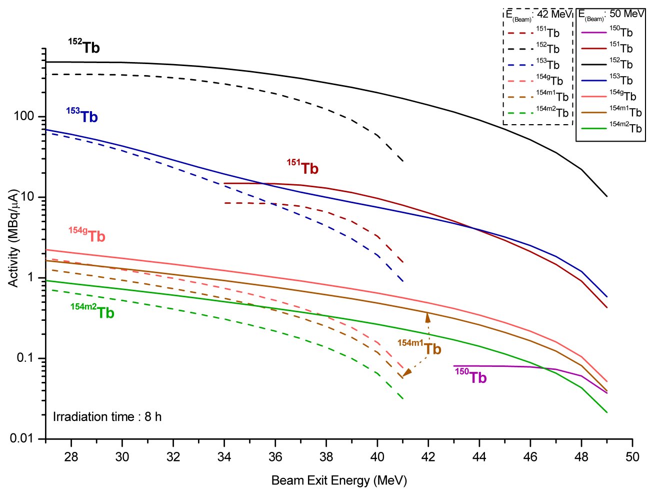

Fig. 8. (Color online) 1 μA beam current and 8 hours of irradiation with 42 MeV (dashed line) and 50 MeV (solid line) beam energy and ^{152}Tb activity with respect to target thickness. Target thickness is given in terms of beam exit energy.

mum activity obtained for ^{150}Tb is 0.8 MBq/μA."

B. The production of ^{155}Tb with ^{153}Eu target

Upon analysis of the production of ^{155}Tb by the reaction ^{153}Eu(α,2n)^{155}Tb, it was observed that the isotopic fraction for ^{155}Tb showed a gradual decrease as the beam energy increased. As illustrated in Figure 9, the irradiation of the enriched ^{153}Eu target for eight hours with a beam energy of 31 MeV and a beam exit energy of 17 MeV results in the production of ^{155}Tb with a 90% isotopic fraction. Under these conditions, a 37.3 MBq activity will be obtained with a 1 μA beam current. The reaction cross sections for the dominant

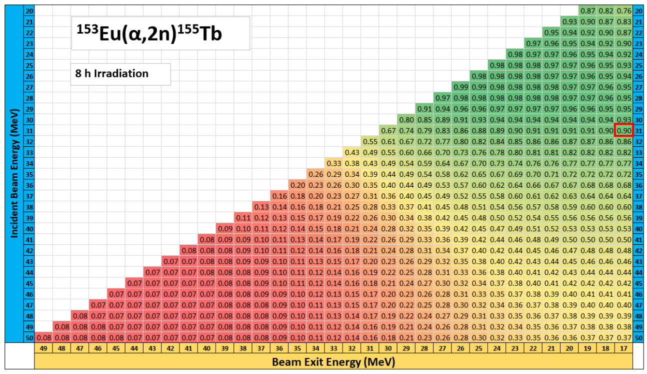

Fig. 9. (Color online) The isotopic fraction of ^{155}Tb with respect to beam energy and target thickness was determined following irradiation with an enriched ^{153}Eu target at a beam current of 1 μA for 8 hours. The target thickness is expressed in terms of the beam energy leaving the target. The beam profile was assumed to be 1 cm^2.

products formed as a consequence of irradiation with the enriched ^{153}Eu target are presented in Figure 10.

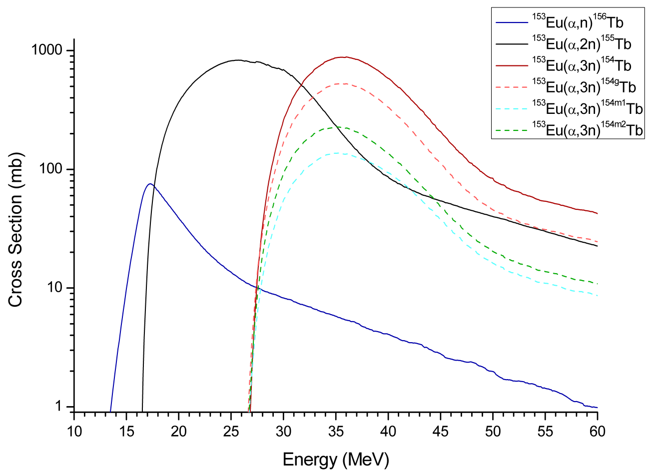

Fig. 10. (Color online) Calculated reaction cross section for the ^{153}Eu target. The dashed lines show the cross section of the ground and two metastable states for reaction ^{153}Eu(α,3n)^{154g,m1,m2}Tb.

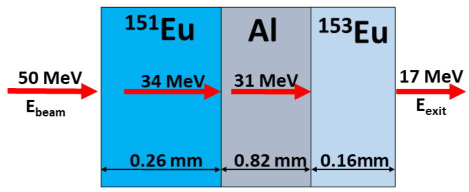

Fig. 11. (Color online) Target design to produce both ^{152}Tb and ^{155}Tb at the same time.

This process allows for the production of both ^{152}Tb and ^{155}Tb isotopes simultaneously. By employing a target design analogous to that depicted in Figure 11, it is possible to generate ^{152}Tb at high energies and ^{155}Tb at low energies. The

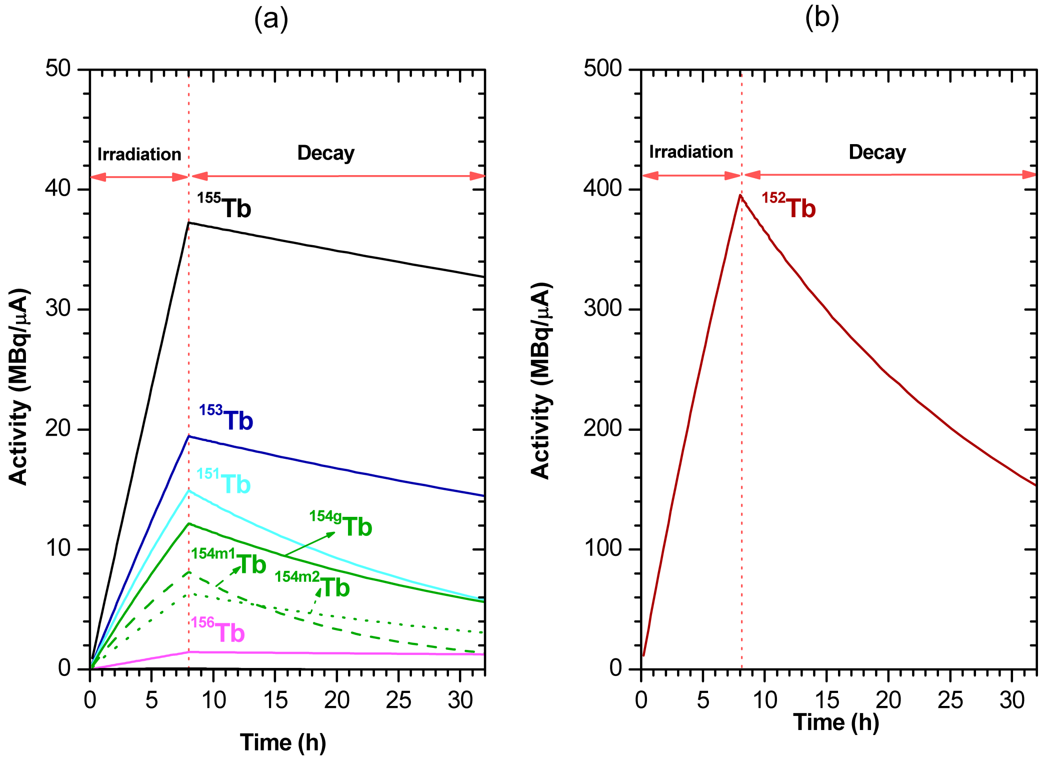

Fig. 12. (Color online)The activity of isotopes formed as a result of 1 μA beam current and 8 hours of irradiation using the target design in Figure 11 and decayed 24 hours after irradiation. (a) For the ^{151}Tb, ^{153}Tb, ^{154g,m1,m2}Tb, ^{155}Tb, and ^{156}Tb (b) for the ^{152}Tb.

utilization of an Al energy gradient is an effective method for minimizing contamination from other isotopes in the intermediate region, thereby reducing both irradiation time and production costs. The required thickness of the Al energy degrader for the purpose of decreasing the beam energy from 34 MeV to 31 MeV was determined through the utilization of the ThiMeT code [56]. Figure 12 illustrates the activities resulting from 8 hours of irradiation and 24 hours of decay, as represented by the proposed target design.

IV. CONCLUSION

A computer code using statistical Hauser-Feshbach approach was used in order to determine the most compatible theoretical results with the experimental data. The reaction cross sections were calculated with TALYS code for a total of 432 different combinations of eight optical potential, six level density and nine strength function models. The calculations closest to the experimental results are those obtained with the combinations of MP-238, which is determined by TLU method. That is, the optical model potential of McFadden and Satchler [29] , Generalised superfluid energy level density model by Ignatyuk et al. [37, 38] and the strenght function model of Gogny D1M HFB+QRPA by Martini et al. [50]. The ^{153}Eu(α,2n)^{155}Tb reaction, for which no experimental cross-section data is available in the literature, was the subject of an in-depth study. The predicted cross-section values allowed us to calculate ^{155}Tb production for the first time.

The TLU method is capable of identifying the most optimal parameter model for predicting reaction cross sections that align with experimental data. In recent times, a considerable number of studies have employed the chi-square test in this field [57]. The TLU method represents a distinct and straightforward approach that could be utilized in future studies.

In order to theoretically determine the medical isotope production parameters, it is necessary to have a good understanding of the cross section, stopping power, and decay parameters. The cross sections derived in this investigation are adequately corroborated by empirical data, and the parameters governing the observed decay are well documented. Currently, there is no experimental data available regarding the stopping power of alpha particles in Eu. Consequently, theoretical calculations must be used as a basis for the determination of these parameters.

Using ^{151}Eu target with 50 MeV beam energy and 34 MeV exit energy, ^{152}Tb with 83% isotopic fraction and 395 MBq/μA activity can be produced. Similarly, ^{155}Tb with 90% isotopic fraction and 37.3 MBq/μA activity can be produced using ^{153}Eu target with 31 MeV beam energy and 17 MeV exit energy. A target design analogous to that depicted in Figure 11 was employed to produce ^{152}Tb with an activ-

ity of 395 MBq/μA and 37.3 MBq/μA of ^{155}Tb, respectively, utilizing a beam energy of 50 MeV. It should be noted that the aforementioned calculations were conducted with a beam current of 1 μA, and thus, the calculated activities will increase in direct proportion to the increase in beam current. It is possible to modify the ratio of ^{152}Tb and ^{155}Tb by allowing the decay of ^{152}Tb.

Further investigations with greater diversity and complexity can be conducted using the proposed model combination. However, more precise measurements of experimental cross sections over a broader energy range would enhance theoretical investigations. It is therefore imperative to employ the thin target activation method in order to obtain precise cross-section measurements, which are crucial for the analysis of the reactions of interest.

---

[1] Naskar, N., Lahiri, S. (2021). Theranostic Terbium Radioisotopes: Challenges in Production for Clinical Application. Frontiers in Medicine, 8. doi: 10.3389/fmed.2021.675014

[2] Müller, C., Singh, A., Umbricht, C. A., Kulkarni, H. R., Johnston, K., Benešová, M., Senftleben, S., Müller, D., Vermeulen, C., Schibli, R., Köster, U., Van Der Meulen, N. P., Baum, R. P. (2019). Preclinical investigations and first-in-human application of 152Tb-PSMA-617 for PET/CT imaging of prostate cancer. EJNMMI Research, 9(1). doi: 10.1186/s13550-019-0538-1

[3] Lehenberger, S., Barkhausen, C., Cohrs, S., Fischer, E., Grünberg, J., Hohn, A., Köster, U., Schibli, R., Türler, A., Zhernosekov, K. (2011). The low-energy β^- and electron emitter 161Tb as an alternative to 177Lu for targeted radionuclide therapy. Nuclear Medicine and Biology, 38(6), 917–924. doi: 10.1016/j.nucmedbio.2011.02.007

[4] Maiti, M. (2011). New measurement of cross sections of evaporation residues from the natPr+12C reaction: A comparative study on the production of. Physical Review. C, 84(4). doi: 10.1103/physrevc.84.044615

[5] Qaim, S. M., Scholten, B., Neumaier, B. (2018). New developments in the production of theranostic pairs of radionuclides. Journal of Radioanalytical and Nuclear Chemistry, 318(3), 1493–1509. doi: 10.1007/s10967-018-6238-x

[6] Beyer, G. J., Comor, J. J., Dakovic, M., Soloviev, D., Tamburella, C., Hagebo, E., Allan, B., Dmitriev, S. N., Zaitseva, N. G. (2002). Production routes of the alpha emitting 149Tb for medical application. Radiochimica Acta, 90(5), 247–252. doi: 10.1524/ract.2002.90.$5_2$002.247

[7] Moiseeva, A. N., Aliev, R. A., Unezhev, V. N., Zagryadskiy, V. A., Latushkin, S. T., Aksenov, N. V., Gustova, N. S., Voronuk, M. G., Starodub, G. Y., Ogloblin, A. A. (2020). Cross section measurements of 151Eu(3He,5n) reaction: new opportunities for medical alpha emitter 149Tb production. Scientific Reports, 10(1). doi: 10.1038/s41598-020-57436-6

[8] Webster, B., Ivanov, P., Russell, B., Collins, S., Stora, T., Ramos, J. P., Köster, U., Robinson, A. P., Read, D. (2019). Chemical Purification of Terbium-155 from Pseudo-Isobaric Impurities in a Mass Separated Source Produced at CERN. Scientific Reports, 9(1). doi: 10.1038/s41598-019-47463-3

[9] Vermeulen, C., Steyn, G., Szelecsényi, F., Kovács, Z., Suzuki, K., Nagatsu, K., Fukumura, T., Hohn, A., Van Der Walt, T. (2012). Cross sections of proton-induced reactions on Gd with special emphasis on the production possibilities of 152Tb and 155Tb. Nuclear Instruments and Methods in Physics Research. Section B, 275, 24–32. doi: 10.1016/j.nimb.2011.12.064

[10] Steyn, G., Vermeulen, C., Szelecsényi, F., Kovács, Z., Hohn, A., Van Der Meulen, N., Schibli, R., Van Der Walt, T. (2014). Cross sections of proton-induced reactions on 152Gd, 155Gd and 159Tb with emphasis on the production of selected Tb radionuclides. Nuclear Instruments and Methods in Physics Research. Section B, 319, 128–140. doi: 10.1016/j.nimb.2013.11.013

[11] R. T. Güray, N. Özkan, C. Yalçın, et al. Measurements of ^{152}Gd(p,γ)^{153}Tb and ^{152}Gd(p,n)^{152}Tb reaction cross sections for the astrophysical γ process. Phys. Rev. C **91**, 055809 (2015). doi: 10.1103/PhysRevC.91.055809

[12] Tárkányi, F., Takács, S., Ditrói, F., Csikai, J., Hermanne, A., Ignatyuk, A. (2014). Activation cross-sections of deuteron induced reactions on natGd up to 50MeV. Applied Radiation and Isotopes, 83, 25–35. https://doi.org/10.1016/j.apradiso.2013.10.010

[13] Gy. Gyürky, Z. Elekes , J. Farkas, et al., Alpha-induced reaction cross section measurements on ^{151}Eu for the astrophysical γ-process. J. Phys. G Nucl. Partic. **37**, 115201 (2010). doi: 10.1088/0954-3899/37/11/115201

[14] Moiseeva, A., Aliev, R., Unezhev, V., Gustova, N., Madumarov, A., Aksenov, N., Zagryadskiy, V. (2021). Alpha particle induced reactions on 151Eu: Possibility of production of 152Tb radioisotope for PET imaging. Nuclear Instruments and Methods in Physics Research. Section B, Beam Interactions With Materials and Atoms, 497, 59–64. doi: 10.1016/j.nimb.2021.04.007

[15] Müller, C., Vermeulen, C., Johnston, K., Köster, U., Schmid, R., Türler, A., Van Der Meulen, N. P. (2016). Preclinical in vivo application of 152Tb-DOTANOC: a radiolanthanide for PET imaging. EJNMMI Research, 6(1). doi: 10.1186/s13550-016-0189-4

[16] Eroğlu, M., Yalçın, C., Güray, R. T. (2023). Investigation of the ^{121}Sb(α,γ)^{125}I reaction cross-section calculations at astrophysical energies. Nuclear Science and Techniques/Nuclear Science and Techniques, 34(11). doi: 10.1007/s41365-023-01301-4

[17] C. Yalçın, The cross section calculation of ^{112}Sn(α,γ)^{116}Te reaction with different nuclear models at the astrophysical energy range. Nucl. Sci. Tech. **28**, 113 (2017). doi: 10.1007/s41365-017-0267-y

[18] R. Baldık, A. Yılmaz, A study on the excitation functions of ^{60,62}Ni(α,n), ^{60,61}Ni(α,2n), ^{58,64}Ni(α,p), ^{nat}Ni(α,x) reactions. Nucl. Sci. Tech. **29**, 156 (2018). doi: 10.1007/s41365-018-0500-3

[19] J.H Luo, J.C. Liang, L. Jiang, et al., Measurement of ^{134}Xe(n,2n)^{133m,g}Xe reaction cross sections in 14-MeV region with detailed uncertainty quantification. Nucl. Sci. Tech. **34**, 4 (2023). doi: 10.1007/s41365-022-01158-z

[20] R. Kruse, C. Borgelt, F. Klawonn, et al., Computational Intelligence (Springer-Verlag, London, 2013), p. 15

[21] Z. Korkulu, N. Özkan, G. G. Kiss, et al. Investigation of α-induced reactions on Sb isotopes relevant to the astrophysical γ process. Phys. Rev. C **97**, 045803 (2018). doi: 10.1103/PhysRevC.97.045803

[22] N. Özkan, R. T. Güray, C. Yalçın, et al., Proton capture reac-

tion cross section measurements on ^{162}Er as a probe of statistical model calculations. Phys. Rev. C **96**, 045805 (2017). doi: 10.1103/PhysRevC.96.045805

[23] C. Yalçın , Gy. Gyürky, T. Rauscher, et al., Test of statistical model cross section calculations for α-induced reactions on ^{107}Ag at energies of astrophysical interest. Phys. Rev. C **91**, 034610 (2015). doi: 10.1103/PhysRevC.91.034610

[24] R. T. Güray, N. Özkan, C. Yalçın, et al., Measurements of proton-induced reaction cross sections on ^{120}Te for the astrophysical p process. Phys. Rev. C **80**, 035804 (2009). doi: 10.1103/PhysRevC.80.035804

[25] C. Yalçın , R. T. Güray, N. Özkan, et al., Odd p isotope ^{113}In: Measurement of α-induced reactions. Phys. Rev. C **79**, 065801 (2009). doi: 10.1103/PhysRevC.79.065801

[26] Ditroi, F., Takacs, S., Tarkanyi, F., Reichel, M., Scherge, M., Gerve, A. (2006). Thin layer activation of large areas for wear study. Wear, 261(11–12), 1397–1400.

[27] A. J. Koning, S. Hilaire, S. Goriely, (2023). TALYS: modeling of nuclear reactions. European Physical Journal. A, 59(6) doi: 10.1140/epja/s10050-023-01034-3

[28] S. Watanabe, High energy scattering of deuterons by complex nuclei. Nucl. Phys. **8**, 484 (1958). doi: 10.1016/0029-5582(58)90180-9

[29] L. McFadden, G. R. Satchler, Optical-model analysis of the scattering of 24.7 MeV alpha particles. Nucl. Phys. **84**, 177 (1966). doi: 10.1016/0029-5582(66)90441-X

[30] P. Demetriou, C. Grama and S. Goriely, Improved global α-optical model potentials at low energies. Nucl. Phys. A **707**, 253 (2002). doi: 10.1016/S0375-9474(02)00756-X

[31] V. Avrigeanu, M. Avrigeanu, and C. Manailescu, Further explorations of the α-particle optical model potential at low energies for the mass range A≈45-209. Phys. Rev. C **90**, 044612 (2014). doi: 10.1103/PhysRevC.90.044612

[32] M. Nolte, H. Machner, and J. Bojowald, Global optical potential for α particles with energies above 80 MeV. Phys. Rev. C **36**, 1312 (1987). doi: 10.1103/PhysRevC.36.1312

[33] V. Avrigeanu, P. E. Hodgson, M. Avrigeanu, Global optical potentials for emitted alpha particles. Phys. Rev. C **49**, 2136 (1994). doi: 10.1103/PhysRevC.49.2136

[34] A. Gilbert, A. G. W. Cameron, A composite nuclear-level density formula with shell corrections. Can. J. Phys. **43**, 1446 (1965). doi: 10.1139/p65-139

[35] W. Dilg, W. Schantl, H. Vonach, et al., Level density parameters for the back-shifted fermi gas model in the mass range 40 $< A < 250$. Nucl. Phys. A **217**, 269 (1973). doi: 10.1016/0375-9474(73)90196-6

[36] P. Demetriou, S. Goriely, Microscopic nuclear level densities for practical applications. Nucl. Phys. A **695**, 95 (2001). doi: 10.1016/S0375-9474(01)01095-8

[37] A.V. Ignatyuk, K.K. Istekov, G.N. Smirenkin, Sov. J. Nucl. Phys. **29**, 450 (1979)

[38] A. V. Ignatyuk, J. L. Weil, S. Raman, et al., Density of discrete levels in 116Sn. Phys. Rev. C **47**, 1504 (1993). doi: 10.1103/PhysRevC.47.1504

[39] S. Goriely, S. Hilaire and A.J. Koning, Improved microscopic nuclear level densities within the Hartree-Fock-Bogoliubov plus combinatorial method. Phys. Rev. C **78**, 064307 (2008). doi: 10.1103/PhysRevC.78.064307

[40] S. Hilaire, S. Goriely, Global microscopic nuclear level densities within the HFB plus combinatorial method for practical applications. Nucl. Phys. A **779**, 63 (2006). doi: 10.1016/j.nuclphysa.2006.08.014

[41] S. Hilaire, M. Girod, S. Goriely et al., Temperature-dependent combinatorial level densities with the D1M Gogny force. Phys. Rev. C **86**, 064317 (2012). doi: 10.1103/PhysRevC.86.064317

[42] J. Kopecky, M. Uhl and R.E. Chrien, Radiative strength in the compound nucleus ^{157}Gd. Phys. Rev. C **47**, 312 (1993). doi: 10.1103/PhysRevC.47.312

[43] J. Kopecky, M. Uhl, Test of gamma-ray strength functions in nuclear reaction model calculations. Phys. Rev. C **41**, 1941 (1990). doi: 10.1103/PhysRevC.41.1941

[44] D.M. Brink, Individual particle and collective aspects of the nuclear photoeffect. Nucl Phys **4**, 215 (1957). doi: 10.1016/0029-5582(87)90021-6

[45] P. Axel, Electric Dipole Ground-State Transition Width Strength Function and 7-Mev Photon Interactions. Phys. Rev. **126**, 671 (1962). doi: 10.1103/PhysRev.126.671

[46] S. Goriely and E. Khan, Large-scale QRPA calculation of E1-strength and its impact on the neutron capture cross section. Nucl. Phys. A **706**, 217 (2002). doi: 10.1016/S0375-9474(02)00860-6

[47] S. Goriely, E. Khan, and M. Samyn, Microscopic HFB + QRPA predictions of dipole strength for astrophysics applications. Nucl. Phys. A **739**, 331 (2004). doi: 10.1016/j.nuclphysa.2004.04.105

[48] S. Goriely, Radiative neutron captures by neutron-rich nuclei and the r-process nucleosynthesis. Phys. Lett. B **436**, 10 (1998). doi: 10.1016/S0370-2693(98)00907-1

[49] D. P. Arteaga, P. Ring, Relativistic random-phase approximation in axial symmetry. Phys. Rev. C **77**, 034317 (2008). doi: 10.1103/PhysRevC.77.034317

[50] M. Martini, S. Hilaire, S. Goriely, et al., Improved Nuclear Inputs for Nuclear Model Codes Based on the Gogny Interaction. Nucl. Data Sheets **118**, 273 (2014). doi: 10.1016/j.nds.2014.04.056

[51] S. Hilaire, M. Girod, S. Goriely et al., Temperature-dependent combinatorial level densities with the D1M Gogny force. Phys. Rev. C **86**, 064317 (2012). doi: 10.1103/PhysRevC.86.064317

[52] V. Plujko, O. Gorbachenko, K, Solodovnyk, Description of nuclear photoexcitation by Lorentzian expressions for electric dipole photon strength function. Eur. Phys. J. A **55**, 1-12 (2019). doi: 10.1140/epja/i2019-12899-6

[53] National Nuclear Data Center (NNDC). http://www.nndc.bnl.gov/nudat3. Accessed 11 May 2024.

[54] N. Otuka, S. Takács, Definitions of radioisotope thick target yields. Radiochimica Acta, 103(1), 1–6 (2014). doi: 10.1515/ract-2013-2234

[55] W. R. Leo, Techniques for Nuclear and Particle Physics Experiments. In: Springer Verlag, Berlin (1994).

[56] C. Yalçın (2015). Thickness measurement using alpha spectroscopy and SRIM. Journal of Physics. Conference Series, 590, 012050. hrefhttps://doi.org/10.1088/1742-6596/590/1/012050doi: 10.1088/1742-6596/590/1/012050

[57] P. Mohr, Gy. Gyürky, Zs. Fülöp, Statistical model analysis of γ-induced reaction cross sections of ^{64}Zn at low energies. Phys. Rev. C **95**, 015807 (2017). doi: 10.1103/PhysRevC.95.015807